Journal of Materials in Civil Engineering

Segmentation method for enhancing the continuity and integrality of microcracks in concrete fracture XCT image

--Manuscript Draft--

Manuscript Number:	MTENG-12154R2
Full Title:	Segmentation method for enhancing the continuity and integrality of microcracks in concrete fracture XCT image
Manuscript Region of Origin:	CHINA
Article Type:	Technical Paper
Section/Category:	Section A1: Cements and novel binders for concrete (e.g., hydration and microstructure)
Manuscript Classifications:	Concrete; Damage (material); Nondestructive tests
Funding Information:	National Natural Science Foundation of China (U1801254) — Shuxian Hong National Natural Science Foundation of China (51727813) — Prof. Biqin Dong National Natural Science Foundation of China (51925805) — Shuxian Hong Project of Department of Education of Guangdong Province, China (2018KZDXM060) — Prof. Biqin Dong
Abstract:	Abstract: The integrality and connectivity of detected cracks are critical to quantitatively analyzing the fracture patterns of cementitious materials using X-ray computed tomography (XCT). Owing to noise, uneven gray values, pores, and other additions with gray values similar to those of the cracks in the raw images, the image segmentation results of microcracks are always with poor continuity and integrality. In this paper, a sophisticated image processing method is proposed to accurately detect integral microcracks in XCT images, and a reconnecting algorithm is proposed to enhance the continuity and integrality of microcracks in the concrete fracture XCT image. The analysis of XCT images of fractured rubber concrete samples verified that the method could visualize and quantitatively analyze the fracture pattern, demonstrating the method's robustness.
Corresponding Author:	Biqin Dong, Ph.D. Shenzhen University Shenzhen, Guangdong CHINA
Corresponding Author E-Mail:	dongbq@gmail.com
Order of Authors:	Shuxian Hong, Ph.D Chuan Kuang Jianchao Zhang Biqin Dong, Ph.D.
Suggested Reviewers:	Jiangxiong Wei He may be proficient in the content that I have written. Hongyan Ma Very well in the related field. Zhengxian Yang He may be proficient in the content that I have written.

	Luping Tang Author of related paper
	Longyuan Li An Expert in the related field.
Opposed Reviewers:	
Additional Information:	
Question	**Response**
Authors are required to attain permission to re-use content, figures, tables, charts, maps, and photographs for which the authors do not hold copyright. Figures created by the authors but previously published under copyright elsewhere may require permission. For more information see http://ascelibrary.org/doi/abs/10.1061/9780784479018.ch03. All permissions must be uploaded as a permission file in PDF format. Are there any required permissions that have not yet been secured? If yes, please explain in the comment box.	No
ASCE does not review manuscripts that are being considered elsewhere to include other ASCE Journals and all conference proceedings (see next question for expanded conference proceeding requirements). Is the article or parts of it being considered for any other publication? If your answer is yes, please explain in the comments box below.	No
Each submission to ASCE must stand on its own and represent significant new information, which may include disproving the work of others. While it is acceptable to build upon one's own work or replicate other's work, it is not appropriate to fragment the research to maximize the number of manuscripts or to submit papers that represent very small incremental changes. ASCE may use tools such as CrossCheck, Duplicate Submission Checks, and Google Scholar to verify that submissions are novel. Does the manuscript constitute incremental work (i.e. restating raw data, models, or conclusions from a previously published study)?	No

Authors are expected to present their papers within the page limitations described in <u>Publishing in ASCE Journals: A Guide for Authors</u>. Technical papers and Case Studies must not exceed 30 double-spaced manuscript pages, including all figures and tables. Technical notes must not exceed 7 double-spaced manuscript pages. Papers that exceed the limits must be justified. Grossly over-length papers may be returned without review. Does this paper exceed the ASCE length limitations? If yes, please provide justification in the comments box below.	No
All authors listed on the manuscript must have contributed to the study and must approve the current version of the manuscript. Are there any authors on the paper that do not meet these criteria? If the answer is yes, please explain in the comments.	No
Was this paper previously declined or withdrawn from this or another ASCE journal? If so, please provide the previous manuscript number and explain what you have changed in this current version in the comments box below. You may upload a separate response to reviewers if your comments are extensive.	No
Companion manuscripts are discouraged as all papers published must be able to stand on their own. Justification must be provided to the editor if an author feels as though the work must be presented in two parts and published simultaneously. There is no guarantee that companions will be reviewed by the same reviewers, which complicates the review process, increases the risk for rejection and potentially lengthens the review time. If this is a companion paper, please indicate the part number and provide the title, authors and manuscript number (if available) for the companion papers along with your detailed justification for the editor in the comments box below. If there is no justification provided, or if there is insufficient justification, the papers will be returned without review.	No, this is not a companion paper
If this manuscript is intended as part of a	No

Special Issue or Collection, please provide the Special Collection title and name of the guest editor in the comments box below.	
Recognizing that science and engineering are best served when data aremade available during the review and discussion of manuscripts andjournal articles, and to allow others to replicate and build on workpublished in ASCE journals, all reasonable requests by reviewers formaterials, data, and associated protocols must be fulfilled. If you are restricted from sharing your data and materials, please explain below.	No
Papers published in ASCE Journals must make a contribution to the core body of knowledge and to the advancement of the field. Authors must consider how their new knowledge and/or innovations add value to the state of the art and/or state of the practice. Please outline the specific contributions of this research in the comments box.	The integrality and connectivity of detected cracks are critical to quantitatively analyzing the fracture patterns of cementitious materials using X-ray computed tomography (XCT). Owing to noise, uneven gray values, pores, and other additions with gray values similar to those of the cracks in the raw images, the conventional methods failed to accurately detect continuous microcracks and could not effectively remove the pores and other additions with similar gray values in the final detected images of the cracks. In this paper, a sophisticated image processing method is proposed to accurately detect integral microcracks in XCT images. Following are some specific reasons for making the paper innovative and publishable: 1) The method has better performance in removing pores, especially for some rounded pores with a hollow or notch and the pores connected to the cracks; 2) After processed by the reconnecting algorithm, the final detected cracks are continuous where are often interrupted using the conventional methods, providing integral and continuous structure for further quantitative statistical analysis. The method offers a feasible method to quantitatively analyze fracture characteristics such as the width and length of cracks in studying fracture mechanics.
The flat fee for including color figures in print is $800, regardless of the number of color figures. There is no fee for online only color figures. If you decide to not print figures in color, please ensure that the color figures will also make sense when printed in black-and-white, and remove any reference to color in the text. Only one file is accepted for each figure. Do you intend to pay to include color figures in print? If yes, please indicate which figures in the comments box.	No
Is this article or parts of it already published in print or online in any language? ASCE does not review content already published (see next questions for conference papers and posted theses/dissertations). If your answer is	No

yes, please explain in the comments box below.	
Has this paper or parts of it been published as a conference proceeding? A conference proceeding may be reviewed for publication only if it has been significantly revised and contains 50% new content. Any content overlap should be reworded and/or properly referenced. If your answer is yes, please explain in the comments box below and be prepared to provide the conference paper.	No
ASCE allows submissions of papers that are based on theses and dissertations so long as the paper has been modified to fit the journal page limits, format, and tailored for the audience. ASCE will consider such papers even if the thesis or dissertation has been posted online provided that the degree-granting institution requires that the thesis or dissertation be posted. <p>Is this paper a derivative of a thesis or dissertation posted or about to be posted on the Internet? If yes, please provide the URL or DOI permalink in the comment box below.	No
When submitting a new and revised manuscript, authors are asked to include a Data Availability Statement containing one or more of the following statements, with specific items listed as appropriate. Please select one or more of the statements below that apply to your manuscript. Also, please include the selected statements in a separate "Data Availability Statement" section in your manuscript, directly before the acknowledgments or references. The statement(s) listed in your manuscript should match those you select in your response to this question.	a. Some or all data, models, or code that support the findings of this study are available from the corresponding author upon reasonable request.
If there is anything else you wish to communicate to the editor of the journal, please do so in this box.	No
COPYRIGHT TRANSFER AGREEMENT **I. Authorship Responsibility**	None of the exceptions listed above apply.

To protect the integrity of authorship, only people who have significantly contributed to the research or project and manuscript preparation shall be listed as coauthors. The corresponding author attests to the fact that anyone named as a coauthor has seen the final version of the manuscript and has agreed to its submission for publication. Deceased persons who meet the criteria for coauthorship shall be included, with a footnote reporting date of death. No fictitious name shall be given as an author or coauthor. An author who submits a manuscript for publication accepts responsibility for having properly included all, and only, qualified coauthors.

II. Originality of Content

ASCE respects the copyright ownership of other publishers. ASCE requires authors to obtain permission from the copyright holder to reproduce any material that (1) they did not create themselves and/or (2) has been previously published, to include the authors' own work for which copyright was transferred to an entity other than ASCE. For any figures, tables, or text blocks exceeding 100 words from a journal article or 500 words from a book, written permission from the copyright holder must be obtained and supplied with the submission. Each author has a responsibility to identify materials that require permission by including a citation in the figure or table caption or in extracted text.

More information can be found in the guide "Publishing in ASCE Journals: Manuscript Submission and Revision Requirements" (http://ascelibrary.org/doi/pdf/10.1061/9780784479018.ch05). Regardless of acceptance, no manuscript or part of a

manuscript will be published by ASCE without proper verification of all necessary permissions to re-use. ASCE accepts no responsibility for verifying permissions provided by the author. Any breach of copyright will result in retraction of the published manuscript.

III. Copyright Transfer

ASCE requires that authors or their agents assign copyright to ASCE for all original content published by ASCE. The author(s) warrant(s) that the above-cited manuscript is the original work of the author(s) and has never been published in its present form.

The undersigned, with the consent of all authors, hereby transfers, to the extent that there is copyright to be transferred, the exclusive copyright interest in the above-cited manuscript (subsequently called the “work”) in this and all subsequent editions of the work (to include closures and errata), and in derivatives, translations, or ancillaries, in English and in foreign translations, in all formats and media of expression now known or later developed, including electronic, to the American Society of Civil Engineers subject to the following:

• The undersigned author and all coauthors retain the right to revise, adapt, prepare derivative works, present orally, or distribute the work, provided that all such use is for the personal noncommercial benefit of the author(s) and is consistent with any prior contractual agreement between the undersigned and/or coauthors and their employer(s).

• No proprietary right other than copyright is claimed by ASCE. • This agreement will be rendered null and void if (1) the manuscript is not accepted for publication by ASCE, (2) is withdrawn by the author prior to publication (online or in print), (3) ASCE Open Access is purchased by the author. • Authors may post a PDF of the ASCE-published version of their work on their employers' ***Intranet*** with password protection. The following statement must appear with the work: "This material may be downloaded for personal use only. Any other use requires prior permission of the American Society of Civil Engineers." • Authors may deposit the ***final draft*** of their work in an institutional repository or in their funding body's designated archive upon publication in an ASCE Journal, provided the draft contains a link to the published version at ascelibrary.org, and may request public access 12 months after publication. "Final draft" means the version submitted to ASCE after peer review and prior to copyediting or other ASCE production activities; it does not include the copyedited version, the page proof, a PDF, or full-text HTML of the published version. • Authors may post the ***final draft*** of their work on open, unrestricted Internet sites 12 months after publication in an ASCE Journal, provided the draft contains a link to the published version at ascelibrary.org. Exceptions to the Copyright Transfer policy exist in the following circumstances. Select the appropriate option below to indicate whether you are claiming an exception: • U.S. GOVERNMENT EMPLOYEES:	

Work prepared by U.S. Government employees in their official capacities is not subject to copyright in the United States. Such authors must place their work in the public domain, meaning that it can be freely copied, republished, or redistributed. In order for the work to be placed in the public domain, ALL AUTHORS must be official U.S. Government employees. If at least one author is not a U.S. Government employee, copyright must be transferred to ASCE by that author.

• CROWN GOVERNMENT COPYRIGHT: Whereby a work is prepared by officers of the Crown Government in their official capacities, the Crown Government reserves its own copyright under national law. If ALL AUTHORS on the manuscript are Crown Government employees, copyright cannot be transferred to ASCE; however, ASCE is given the following nonexclusive rights: (1) to use, print, and/or publish in any language and any format, print and electronic, the above-mentioned work or any part thereof, provided that the name of the author and the Crown Government affiliation is clearly indicated; (2) to grant the same rights to others to print or publish the work; and (3) to collect royalty fees. ALL AUTHORS must be official Crown Government employees in order to claim this exemption in its entirety. If at least one author is not a Crown Government employee, copyright must be transferred to ASCE by that author.

• WORK-FOR-HIRE: Privately employed authors who have prepared works in their official capacity as employees must also transfer copyright to ASCE; however, their employer retains the rights to revise, adapt, prepare derivative works, publish, reprint, reproduce, and distribute the work provided that such use is for the promotion of its business enterprise and does not imply the endorsement of ASCE. In this instance, an authorized agent from the authors' employer must sign the form below.

• **U.S. GOVERNMENT CONTRACTORS**: Work prepared by authors under a contract for the U.S. Government (e.g., U.S. Government labs) may or may not be subject to copyright transfer. Authors must refer to their contractor agreement. For works that qualify as U.S. Government works by a contractor, ASCE acknowledges that the U.S. Government retains a nonexclusive, paid-up, irrevocable, worldwide license to publish or reproduce this work for U.S. Government purposes only. This policy DOES NOT apply to work created with U.S. Government grants.	
Please type your name below to complete the copyright transfer agreement. This will serve as your digital signature. *I, the corresponding author, confirm that the authors listed on the manuscript are aware of their authorship status and qualify to be authors on the manuscript according to the guidelines above.* *I, the corresponding author, confirm that the content, figures, drawings, charts, photographs, and tables in the submitted work are either original work created by the authors listed on the manuscript or work for which permission to re- use has been obtained from the creator.* *I, the corresponding author, acting with consent of all authors listed on the manuscript, hereby transfer copyright or claim exemption to transfer copyright of the work as indicated above to the American Society of Civil Engineers.* as follow-up to "**COPYRIGHT TRANSFER AGREEMENT** **I. Authorship Responsibility**	Biqin Dong

To protect the integrity of authorship, only people who have significantly contributed to the research or project and manuscript preparation shall be listed as coauthors. The corresponding author attests to the fact that anyone named as a coauthor has seen the final version of the manuscript and has agreed to its submission for publication. Deceased persons who meet the criteria for coauthorship shall be included, with a footnote reporting date of death. No fictitious name shall be given as an author or coauthor. An author who submits a manuscript for publication accepts responsibility for having properly included all, and only, qualified coauthors.

II. Originality of Content

ASCE respects the copyright ownership of other publishers. ASCE requires authors to obtain permission from the copyright holder to reproduce any material that (1) they did not create themselves and/or (2) has been previously published, to include the authors' own work for which copyright was transferred to an entity other than ASCE. For any figures, tables, or text blocks exceeding 100 words from a journal article or 500 words from a book, written permission from the copyright holder must be obtained and supplied with the submission. Each author has a responsibility to identify materials that require permission by including a citation in the figure or table caption or in extracted text.

More information can be found in the guide "Publishing in ASCE Journals: Manuscript Submission and Revision Requirements" (http://ascelibrary.org/doi/pdf/10.1061/978

0784479018.ch05). Regardless of acceptance, no manuscript or part of a manuscript will be published by ASCE without proper verification of all necessary permissions to re-use. ASCE accepts no responsibility for verifying permissions provided by the author. Any breach of copyright will result in retraction of the published manuscript.

III. Copyright Transfer

ASCE requires that authors or their agents assign copyright to ASCE for all original content published by ASCE. The author(s) warrant(s) that the above-cited manuscript is the original work of the author(s) and has never been published in its present form.

The undersigned, with the consent of all authors, hereby transfers, to the extent that there is copyright to be transferred, the exclusive copyright interest in the above-cited manuscript (subsequently called the “work”) in this and all subsequent editions of the work (to include closures and errata), and in derivatives, translations, or ancillaries, in English and in foreign translations, in all formats and media of expression now known or later developed, including electronic, to the American Society of Civil Engineers subject to the following:

• The undersigned author and all coauthors retain the right to revise, adapt, prepare derivative works, present orally, or distribute the work, provided that all such use is for the personal noncommercial benefit of the author(s) and is consistent with any prior contractual agreement between the undersigned and/or coauthors and their

employer(s). • No proprietary right other than copyright is claimed by ASCE. • This agreement will be rendered null and void if (1) the manuscript is not accepted for publication by ASCE, (2) is withdrawn by the author prior to publication (online or in print), (3) ASCE Open Access is purchased by the author. • Authors may post a PDF of the ASCE-published version of their work on their employers' ***Intranet*** with password protection. The following statement must appear with the work: "This material may be downloaded for personal use only. Any other use requires prior permission of the American Society of Civil Engineers." • Authors may deposit the ***final draft*** of their work in an institutional repository or in their funding body's designated archive upon publication in an ASCE Journal, provided the draft contains a link to the published version at ascelibrary.org, and may request public access 12 months after publication. "Final draft" means the version submitted to ASCE after peer review and prior to copyediting or other ASCE production activities; it does not include the copyedited version, the page proof, a PDF, or full-text HTML of the published version. • Authors may post the ***final draft*** of their work on open, unrestricted Internet sites 12 months after publication in an ASCE Journal, provided the draft contains a link to the published version at ascelibrary.org. Exceptions to the Copyright Transfer policy exist in the following circumstances. Select the appropriate option below to indicate whether you are claiming an exception:	

• **U.S. GOVERNMENT EMPLOYEES**: Work prepared by U.S. Government employees in their official capacities is not subject to copyright in the United States. Such authors must place their work in the public domain, meaning that it can be freely copied, republished, or redistributed. In order for the work to be placed in the public domain, ALL AUTHORS must be official U.S. Government employees. If at least one author is not a U.S. Government employee, copyright must be transferred to ASCE by that author.

• **CROWN GOVERNMENT COPYRIGHT**: Whereby a work is prepared by officers of the Crown Government in their official capacities, the Crown Government reserves its own copyright under national law. If ALL AUTHORS on the manuscript are Crown Government employees, copyright cannot be transferred to ASCE; however, ASCE is given the following nonexclusive rights: (1) to use, print, and/or publish in any language and any format, print and electronic, the above-mentioned work or any part thereof, provided that the name of the author and the Crown Government affiliation is clearly indicated; (2) to grant the same rights to others to print or publish the work; and (3) to collect royalty fees. ALL AUTHORS must be official Crown Government employees in order to claim this exemption in its entirety. If at least one author is not a Crown Government employee, copyright must be transferred to ASCE by that author.

• **WORK-FOR-HIRE**: Privately employed authors who have prepared works in their official capacity as employees must also transfer copyright to ASCE; however, their employer retains the rights to revise, adapt, prepare derivative works, publish, reprint, reproduce, and distribute the work provided that such use is for the promotion of its business enterprise and does not imply the endorsement of ASCE. In this instance, an authorized agent from

the authors' employer must sign the form below. • **U.S. GOVERNMENT CONTRACTORS**: Work prepared by authors under a contract for the U.S. Government (e.g., U.S. Government labs) may or may not be subject to copyright transfer. Authors must refer to their contractor agreement. For works that qualify as U.S. Government works by a contractor, ASCE acknowledges that the U.S. Government retains a nonexclusive, paid-up, irrevocable, worldwide license to publish or reproduce this work for U.S. Government purposes only. This policy DOES NOT apply to work created with U.S. Government grants."	

Segmentation method for enhancing the continuity and integrality of microcracks in concrete fracture XCT image

Shuxian Hong[1], Chuan Kuang[2], Jianchao Zhang[3], Biqin Dong[4]

[1]Associate Professor, Shenzhen University, Shenzhen, 518060, PR China. Email: sxhong@szu.edu.cn

[2]Postgraduate Student, Shenzhen University, Shenzhen, 518060, PR China. Email: kuangchuan2018@email.szu.edu.cn

[3]Doctoral Student, Shenzhen University, Shenzhen, 518060, PR China. Email: zhangjianchao728@163.com

[4]Professor, Shenzhen University, Shenzhen, 518060, PR China (Corresponding author). Email: incise@szu.edu.cn.

Abstract: The integrality and connectivity of detected cracks are critical to quantitatively analyzing the fracture patterns of cementitious materials using X-ray computed tomography (XCT). Owing to noise, uneven gray values, pores, and other additions with gray values similar to those of the cracks in the raw images, the image segmentation results of microcracks are always with poor continuity and integrality. In this paper, a sophisticated image processing method is proposed to detect integral microcracks in XCT images accurately, and a reconnecting algorithm is proposed to enhance the continuity and integrality of microcracks in the concrete fracture XCT image. The analysis of XCT images of fractured rubber concrete samples verified that the method could visualize and quantitatively analyze the fracture pattern, demonstrating the method's robustness.

Keywords: crack detection; pore removal; connectivity; X-ray microcomputed tomography

1. Introduction

Fracture damage has caused considerable losses in many fields in recent years and has attracted researchers' attention. The quantitative analysis of cracks is an important method to study fracture mechanics in cementitious materials (Brahma et al. 1987; Fukumura et al. 2017; Kim et al. 2020; Weng et al. 2019; Yang et al. 2018; Zhao et al. 2012). In recent years, X-ray computed tomography (XCT) as a non-destructive technique has been widely used to in-situ track the fracture process in cementitious materials and visualize the cracks in three dimensions. Integral and connected cracks in the raw XCT images are still difficult to detect because of the presence of noise, uneven gray values caused by beam hardening artifacts (Boas and Fleischmann 2012; Maki et al. 1999), pores, and other additions with gray values similar to those of the cracks, especially microcracks existing in concrete mixed with rubber particles or fibers. The interruption of the detected cracks will destroy the connectivity, negatively affecting the fracture investigation (Krajcinovic 1998; Zhou et al. 2011) due to a higher number and shorter lengths of cracks.

Digital volume correlation (DVC) is a non-contact method to measure the internal three-dimensional displacement field and strain field, particularly in conjunction with XCT (Germaneau et al. 2007). The DVC technique obtains the displacement vector by tracking the change of the gray value between a reference sub-volume image and the deformed sub-volume image. The optimal sub-volume size is dependent on the size of speckles and is generally set to three times the diameter of speckles (Hong et al. 2020b), which means that the resolution of displacement images obtained by DVC is much lower than XCT images. Thus, DVC technology can hardly extract microcrack images with high resolution from the displacement images for sophisticated analysis of cementitious materials' fracture features.

Previous studies have made some progress after investigating the fracture of cementitious materials via image processing methods (Wang et al. 2020; Yang et al. 2017; Yang et al. 2020), but accurate detection of integral and continuous cracks for further analysis remains a

significant challenge. As a primary image segmentation method, grayscale thresholding algorithms, including local thresholding algorithm and global thresholding algorithm, continue to be widely used to calculate the grayscale threshold for distinguishing the cracks from the cement, aggregates, and other additions in the XCT images of fractured cementitious materials (Hong et al. 2019; Loeffler et al. 2018; Skarżyński and Tejchman 2016). However, due to the effects of noise, uneven gray values, and low contrast on the cracks' detection, thresholding algorithms ignore some of the microcracks and detect interrupted cracks in sectional images (Hong et al. 2020a; Hong et al. 2019; Yang et al. 2017). Moreover, the roundness index has been used to distinguish cracks from pores in the binary images, and the isolated pores were removed (Hong et al. 2019). However, there were still some pores connected to cracks in the final detected cracks' images, and the cracks were not integral. Many algorithms based on the curvilinear structure's geometric properties have been proposed to detect retinal blood vessels without interruption (Chen et al. 2016; Xie et al. 2019; Zhang et al. 2018). However, the algorithms are not suitable for the cracks in cementitious materials because they are not smooth and have many bifurcations, which are different from the smooth and well-oriented vessels. Therefore, the conventional methods failed to detect continuous microcracks accurately from XCT images and could not effectively remove all the pores and additions with similar gray values in the cracks' final detected images.

To resolve this problem, this paper proposes a sophisticated image processing method consisting of five steps: background correction, enhancement, binarization, shape filter, and reconnection. The connected pores are suppressed by the enhancement, while the isolated pores/rubbers are removed by the shape filter based on the roundness index. Finally, the interrupted cracks are reconnected using the proposed algorithm. To demonstrate the robustness of the proposed method, the fracture patterns of rubber concrete were investigated. As rubber concrete is a heterogeneous multiphase quasi-brittle composite material (Akono et al. 2018), it has highly complex fracture images and thinner cracks because of its higher ductile, with a lot of microcracks and pores/rubbers.

2. Experiment

Samples with different rubber contents (5%, 10%, 15%) were prepared and then tested using in situ loading XCT under the ultimate load. The raw XCT images were then obtained using the image acquisition process as described in detail in our previous study (Hong et al. 2020a). Each sample was scanned by the in-situ XCT (XRadia Micro XCT-400, USA). As shown in Table 1, several key parameters were used in the test. The specimens were loaded in an in situ loading device (DEBEN, Mechanical Operation V1.0, UK) attached to the XCT instrument (XRadia Micro XCT-400, USA) and the loading speed was 0.1 mm/min. XCT scanning was performed at loads of 0%, 50%, and 90% of the ultimate load. Finally, the specimen was loaded to destruction (ultimate load), and the last scan was performed. The ultimate loads of the samples with different rubber contents were shown in Table 2.

Each sectional XCT image had a size of 1024×1024×1000 voxels, and the gray values varied from 0 to 65535. As shown in Fig. 1, the gray values in a typical sectional raw XCT image were uneven, owing to the beam hardening artifact (Boas and Fleischmann 2012; Maki et al. 1999). Moreover, unhydrated cement, pores, rubber particles, and cracks, with high or low gray values, were randomly distributed in the image, whose contrast was low, aggravating the unevenness. In addition, some pores were connected to the cracks, as shown in area A# in Fig. 1.

3. Image processing algorithm

Owing to the unevenness mentioned above, low contrast of the region between the cracks and the cement matrix in the image, and blurred boundary of the sample, cracks were often detected with interrupted and incomplete structure. Moreover, it was difficult to remove the pores connected to the cracks without destroying the connectivity. To solve the above problems, as shown in Fig. 2, a new image processing algorithm involving the following steps is proposed to extract cracks:

1) The raw image F is preprocessed by subtracting the air outside the sample and normalizing gray values of the sample area, and the image F_1 is obtained.

2) The structures with low gray values in F_1 are obtained, and the response map F_2 of cracks, pores, and rubber particles is obtained.

3) The image F_2 is binarized using an adaptive Otsu's method to remove the pores and rubber particles with a lower response than the cracks, and the binary image F_3 is obtained.

4) The cracks from F_3 are filtered using the shape index, and the image F_4 of the cracks is obtained.

5) The interrupted cracks in F_4 are reconnected, and the image F_5 of the reconnected cracks is obtained.

Each of the steps is described in detail in the following sections. The procedure is implemented with our in-house code, which is developed based on Matlab.

3.1 Preprocessing

A large amount of noise caused by the beam hardening artifact blurs the sample boundary (Fig. 1), especially where the cracks are connected to the outside air, as shown in area B# in Fig. 1. A preprocessing method was applied to the raw image by identifying the sample's accurate boundary to obtain a clear sample image where the air outside the sample is removed. The method has been described in our previous study (Hong et al. 2019).

The grayscale histogram of the XCT image shows a typical bimodal form, as shown in Fig. 3. The background outside the specimen belongs to the gas phase, and its gray value around the left peak is lower than that of the solid phase around the right peak, so a grayscale threshold can be used here to distinguish the background from the solid phase. The paper used Otsu thresholding algorithm (Otsu 1979) to choose the optimal threshold by maximizing the between-class variance of the gray values of the solid phase and the background. After using the Otsu’s method, some cracks were incorrectly connected to the background, as shown in Fig.

4 (a). In the paper, a closure operation was used here to identify the actual boundary (Hong et al. 2019), and the result is shown in Fig. 4(b).

Then, max-min normalization was applied to the gray values of the sample to improve the contrast. Moreover, the external background was set to white with a gray value of 65535 to distinguish the background from the cracks, pores, and rubber particles in the subsequent image processing. Finally, the region outside the raw sample image was cleared, while the contrast was improved, as shown in Fig. 5. The preprocessing removed the gas phase outside the sample with an area of $1.0445\times108\ \mu m^2$ but did not change the phases in the sample.

3.2 Enhancement

Although the above preprocessing operation improved the contrast, the phenomenon of uneven brightness still existed, making it difficult to distinguish some pixels in the cracks from the cement matrix. To study the effect of the unevenness on the detection, the image in Fig. 6(a) was binarized using the adaptive Otsu's method (Farrahi Moghaddam and Cheriet 2010), which will be introduced in the next section. As a result, shown in Fig. 6(b), the crack on P_1–P_2 was interrupted at point P_3, where the gray value was close to that of the cement matrix. Therefore, the uneven brightness will cause the interruption of some detected cracks. In addition, it is difficult to remove the pores connected to the cracks because their gray values are similar to those of the cracks.

A solution to extract relatively integral cracks is to enhance the structures with low gray values to avoid unevenness. Accordingly, in this study, an enhancement function based on Hessian eigenvalues (Jerman et al. 2016) was applied for its advantage in enhancing elongated structures and round structures. The enhancement based on the eigenvalues of the Hessian matrix is performed through the following function:

$$v_p = \begin{cases} 0 & \lambda_2 \le 0 \cup \lambda_\rho \le 0 \\ 1 & \lambda_2 \ge \lambda_\rho/2 > 0 \\ \lambda_2^2(\lambda_\rho - \lambda_2)\left[\frac{3}{\lambda_2 + \lambda_\rho}\right]^3 & otherwise \end{cases}, \quad (1)$$

where λ_2 is the maximum of the two eigenvalues of the Hessian matrix at each point in a 2D image, and the output value v_p is the possibility of elongated structures or round structures at each point. The parameter λ_ρ is calculated using the following function:

$$\lambda_\rho(s) = \begin{cases} \lambda_2 & \lambda_2 > \max \lambda_2(\mathrm{x}, s) \\ \tau \max \lambda_2(\mathrm{x}, s) & 0 < \lambda_2 \le \max \lambda_2(\mathrm{x}, s) \\ 0 & otherwise \end{cases}, \quad (2)$$

where τ is a threshold between 0 and 1 to clear out the points of no interest. All the calculations in Eq. 1–2 are computed in a window with a size of $s \times s$ pixels centered around the point x in the image.

To demonstrate the enhancement performance, the preprocessed image in Fig. 5 was processed in Eq. 1–2, and then a response map of cracks, rubber particles, and pores was obtained as a gray image (Fig. 7a). After the enhancement, the pore connected to the crack in area A# in Fig. 7(b) was suppressed while preserving the round edge (Fig. 7b), which could be removed using the adaptive Otsu's method (Farrahi Moghaddam and Cheriet 2010) in the next binarization when the interruption occurred at the junction with the crack because of the different gray values from that of the crack (Fig. 7(c)). Moreover, the crack on line P_1–P_2 after the enhancement in Fig. 7(b) had significantly higher gray values than that of the cement matrix; especially, the point P_3, which was interrupted in Fig. 7(c), was connected in the binary result after the enhancement (Fig. 7(c)). Hence, the enhancement can significantly improve the contrast and suppress the pores connected to the cracks, making crack detection easier.

3.3 Binarization

The elongated and round structures, rubber particles, pores, and cracks, were retained, while an uneven variation was also manifested after the enhancement. In Fig. 7(a), the gray values denote the enhancement function's response in Eq. 1 at pixels. Hence, the histogram of the gray values in the enhanced image, as illustrated in Fig. 8, can be used to study the distribution of the probability of the pixels belonging to cracks, pores, and rubber particles.

In Fig. 8, the region near value 0 has no cracks, pores, and rubber particles, while the region near value 1 has them. Therefore, a suitable threshold can be used to identify cracks, pores, and rubber particles. Considering the undesirable uneven variation in Fig. 7(a), the global thresholding algorithm is not suitable for detecting dark objects, including the cracks. An adaptive thresholding algorithm based on Otsu's method (Farrahi Moghaddam and Cheriet 2010) was applied to solve this problem. That is, the adaptive threshold for each point on the enhanced image in Fig. 7(a) was calculated by applying Otsu's method (Otsu 1979) to the gray values of the pixels in the window with a size of $s \times s$ pixels centered at the point. To ensure cracks did not entirely occupy each window, the paper set the window slightly larger than the cracks' maximum width. Cracks, pores, and rubber particles in the raw image (Fig. 7a) were finally obtained through the method as shown in the binary image (Fig. 9b).

The gas-phase part in the sample area consists of pores and cracks represented as the foreground in the binary images. The binary results of the raw XCT image and the enhanced image in Fig. 7(a) are shown in Fig. 9(a)-(b). After the image enhancement, the gas-phase area (Fig. 9(b)) decreases by 2.41%, from 1.4925 $\times 10^7$ μm^2 to 1.4564 $\times 10^7$ μm^2. Meanwhile, the solid-phase area increases by 0.42%, from 8.6135$\times 10^7$ μm^2 to 8.6495 $\times 10^7$ μm^2. The above results can be explained by the fact that the structure of the pores connected to cracks is suppressed in the image enhancement, causing this part to be processed as a non-gas phase part in the binarization. Moreover, the subsequent comparative analysis of different image segmentation methods in section 4.1 indirectly shows that the enhancement does not significantly reduce the extracted cracks' dimensional accuracy.

Fig. 9(b) shows that the cracks were preserved with many pores and rubber particles remaining. Moreover, these pores and rubber particles' values were almost the same as those of the cracks, as shown in Fig. 10 (a), making it difficult to separate them according to their gray values. The elongated cracks had a different shape from the round pores and rubber particles, as shown in Fig. 10(b), so a filter method based on the shape is proposed in the next section.

3.4 Shape filter

To distinguish the cracks from the pores and rubber particles, as shown in Fig. 10(b), a morphology-based roundness index was used, which is defined as follows:

$$p = 4\pi A/L^2, \tag{3}$$

where A is the area of the component and L is the perimeter. The value of the roundness index p is among (0,1]. The closer the value of p is to 1, the more the component tends to be round; the closer the value of p is to 0, the more it tends to be linear. Hence, a suitable threshold p_0 can be used to distinguish between pores and cracks.

However, small round components with a hollow or notch as shown will be identified as cracks if directly calculated using Eq. 1. To correctly distinguish such components, the smallest external convex polygon containing the small components needs to be filled to calculate the roundness index p.

To remove all isolated pores and rubber particles in Fig. 9(b), a shape filter was used, following the steps below, as illustrated in Fig. 11:

1) All the components denoted by R are labeled with the number i (1, 2,…, n) in the binary image F_w.

2) The area value A_i of each component R_i is calculated.

3) The convex hull of R_i is filled if A_i is lower than A_T, and a new component R_i^1 is obtained. If not, let R_i^1 equal R_i.

4) The roundness index p_i of R_i^1 is calculated using Eq. 3.

5) The pixels of R_i in F_w are set as the foreground as cracks if p_i is lower than p_T; otherwise, the pixels are set as the background.

To further illustrate the above filling operation, at step 3, a synthetic hollow round component with a notch was used (Fig. 12a). Using the method described in (Barber et al. 1996), when the component's area was lower than A_T, the convex hull of the component was shaped like the red convex polygon in Fig. 12(b). The filling operation was done by setting the pixels inside the convex hull as the foreground. The pixels on the boundary were set as the foreground if the pixels' inner area is greater than half; otherwise, they were set as the background.

Besides, the threshold A_T of the area for identifying the small components at step 3 was estimated using the following equation:

$$A_T = \pi d^2 \tag{4}$$

where d is a typical width of the wide cracks, about 10 pixels for the samples. The result after many attempts demonstrated that round components could be well removed with a roundness index threshold p_T of 0.7 to obtain the image of the cracks shown in Fig. 13.

However, some cracks obtained by the shape filter (Fig.11) were interrupted after the above series of treatments. To address this shortcoming, a reconnection algorithm is proposed.

3.5 Reconnection

For the filtered cracks in Fig. 13, there are two major kinds of structure discontinuity. As three synthetic discrete components illustrated in Fig. 14, discontinuities occur when there is a

lack of connectivity between the endpoints or branches of each object's centerline. Type B discontinuity occurs when a crack breaks into two in the same direction, while type A occurs when a crack breaks into two cracks, with a specific angle at the bifurcation. Suvadip Mukherjee et al. proposed two reconnecting algorithms according to the two discontinuity types' different characteristics (Mukherjee et al. 2015). Compared with smooth and well-oriented vessels, the cracks were not smooth and had many bifurcations. Thus, the reconnecting algorithm is not suitable for the cracks.

As illustrated in Fig. 14, there will always be one component's endpoint (or tip) and the other component's body when the discontinuity occurs. Accordingly, a new reconnecting algorithm, illustrated in Fig. 15, is proposed based on the two discontinuity types' common characteristic. The algorithm contains the following steps:

1) The components denoted by H are labeled with the number t (1, 2,…, n) in the binary image Q_w of the cracks obtained by the shape filter.

2) The endpoints E_t of the skeleton and the boundary line O_t of each component H_t (t = 1, 2,…, n) are identified.

3) The shortest path LP_{ij} from E_i to O_j (i, j = 1, 2,…, n; $i \neq j$) is found.

4) The pixels on the path LP_{ij} are set as the foreground in Q_w and as the reconnection if the length l_{ij} of LP_{ij} is lower than the threshold l_T (i, j = 1, 2,…, n; $i \neq j$).

At step 2, the components' skeleton can be identified using the thinning methodology (Lam et al. 1992). The outer contour is found by setting each pixel to the background if all its connected neighbors are foreground on the components. At step 3, the shortest path LP_{ij} for two components i and j, which is the path from the ends of the skeleton of component i to the outer contour of component j, is found. Owing to the improvement in the extracted cracks' integrality using the background correction and the enhancement, the disjoint components are not

separated too far apart. Hence, the length l_{ij} of path LP_{ij} can be used to determine whether the two components should be connected, where the threshold l_T is set to the maximal width of the cracks. If the path length is lower than the threshold, the path serves as a line segment to reconnect the two components. As shown in Fig. 16(b–c), the reconnecting algorithm achieved good results for different continuities, including type A and type B; the length threshold l_T used here was 11 pixels. In addition, the components with area lower than A_T were removed as noises.

4. Results and discussion

4.1. Comparison with other segmentation methods

To highlight the effectiveness of the proposed method in detecting cracks in the raw images, its performance was compared with five commonly used threshold segmentation methods in the literature (Doyle 1962; Huang and Wang 1995; Kittler and Illingworth 1986; Otsu 1979; Ridler and Calvard 1978) applied to a typical raw XCT image (Fig. 17a). These methods were combined with the shape filter, whose threshold (0.7) was the same as that of the proposed. As shown in Fig. 17(c–g), the shape filter had good performance in different segmentation results; the pores (gray) and cracks (white) were well distinguished using the shape filter with a threshold of 0.7. In addition, cracks in the raw image were manually marked as a reference. To quantitatively analyze the difference between the methods mentioned above and the real cracks obtained by manual marking, this study defines the characteristic length and width.

As illustrated in Fig. 18, the crack length is obtained by calculating the skeleton line's length (red line). The skeleton line is equally divided into *n* parts, and the crack is vertically divided at each skeleton segment into *n* parts (Fig. 18). The equivalent width of cracks can be calculated in Eq. 5–6.

$$Area \approx \sum_{i=1}^{n} (w_i l_i) \approx \sum_{i=1}^{n} \left(w_i \frac{l}{n} \right) = \frac{l}{n} \times \sum_{i=1}^{n} w_i = l \frac{(\sum_{i=1}^{n} w_i)}{n} = lw, \quad (5)$$

li is the length of the skeleton line part, wi is the width of the crack part, l is the total length of the skeleton line, w is the crack's equivalent width.

$$w = Area/l, \tag{6}$$

where *area* is the crack area.

The maximal and minimal widths were found after each crack's width was calculated using Eq. 6, and the total lengths of the detected cracks are presented in Table 3. As seen in Table 3, the maximal and minimal widths detected by the proposed method are closer to the true value than the widths detected by the conventional methods (Doyle 1962; Huang and Wang 1995; Kittler and Illingworth 1986; Otsu 1979; Ridler and Calvard 1978); this indicates that the method could better detect the edge contour of the crack, while the conventional methods failed. In addition, the total length of cracks extracted by the proposed method is more accurate because the method could extract some small cracks which the conventional methods (Doyle 1962; Huang and Wang 1995; Kittler and Illingworth 1986; Otsu 1979; Ridler and Calvard 1978) could not detect, which is consistent with the results shown in Fig. 17. Moreover, the number of cracks detected by the conventional methods was much higher than the true value, while the proposed method yielded no error. Therefore, the proposed method could retain the cracks' continuity, while the conventional methods interrupted the cracks, owing to the uneven gray values and low contrast. Moreover, the proposed method could detect the cracks more accurately than the conventional methods, as the shape width and length of the detected cracks were very close to those of the manually marked cracks.

4.2. Pore removal performance

In the proposed method, pore removal is completed by the enhancement and shape filter procedures. The raw images' pores have highly similar gray values with the cracks, and some pores are connected to the cracks. Thus, the pore removal performance directly affects crack detection. To further illustrate the pore removal performance, the processing results of three

typical uneven raw image fragments in Fig 19(a–c) were obtained (Fig. 19d–f). The isolated pores in the raw images were distinguished and removed by the shape filter. Moreover, the pores connected to the crack pointed by the arrow in Fig. 19(a–c) were removed in the enhancement procedure. Thus, the proposed method has good pore removal performance, both for the connected and isolated pores.

4.3. Connectivity

Owing to the uneven gray values and low contrast, as shown in Fig. 5, the detected cracks without the reconnection were often interrupted. The interruption also occurred where the pores connected to the cracks were removed. The type B and type A discontinuities were all repaired using the proposed reconnecting algorithm, as shown in Fig. 19(g-i). Consequently, the reconnecting algorithm retained the original connectivity of the cracks.

4.4. Verification of algorithm robustness

To verify the robustness of the proposed algorithm, the method was used to detect the cracks of samples with different rubber contents under the ultimate load, and the detected sectional binarized images were stacked into three-dimensional images, as shown in Fig. 20(a, c, e). The three three-dimensional crack images had significant linear uninterrupted features and no spherical structure, which again indicates that the proposed method can effectively remove pores and retain the connectivity in detecting the cracks. In addition, the cracks in all the samples with different rubber contents had a ring-like shape, and almost all were distributed on the outside of the image (Fig. 20b, d, f); this result matches with the image features of concrete samples when uniaxially loaded to the ultimate load in the existing literature (Di et al. 2018; Meng et al. 2016; Sfer et al. 2002), which has been previously explained by the cyclo-hoop effect described in (Dong et al. 2019).

As shown in Fig. 20, the cracks' three-dimensional geometric characteristics are too complex to calculate the width and length. Therefore, the length of the cracks on the XY

sections at different heights in the loading direction was calculated using the skeleton line in Fig. 18. As illustrated in Fig. 21, with higher rubber content, the number of cracks shorter than 1.2 mm in the sample under the ultimate load increased. The result implies that the rubber's addition improves the ductility of rubber concrete and causes more short cracks, consistent with the previous studies (Li et al. 2018; Taha et al. 2008).

Furthermore, the width of cracks on the XY sections at different heights was calculated in Eq. 6 and counted as shown in Fig. 22. The sample with a higher rubber content had more thin cracks, implying that the incorporated rubber improved the rubber concrete's ductility and made it easier to produce thin cracks (Taha et al. 2008). However, when the rubber content was 15%, the number of cracks with larger width sharply dropped; this may be due to the lower ultimate load of the sample with more rubber (Eldin and Senouci 1994; Huang et al. 2020), making it challenging to produce a wide crack (Ho et al. 2012; Li et al. 2014). The above cracking patterns in the rubber concrete when subjected to uniaxial compression accords with the previous studies (Di et al. 2018; Han et al. 2019; Ho et al. 2012).

5. Conclusion

This paper proposes an image processing method to extract integral and continuous microcracks from complex XCT images of cementitious materials. The conclusions obtained are as follows:

- The proposed method can accurately detect microcracks in uneven noisy low-contrast XCT images.
- The method has good pore removal performance, as illustrated in this study using three typical uneven raw image fragments.
- The final detected cracks obtained using the reconnecting algorithm are continuous, providing a continuous structure for further quantitative statistical analysis.

■ The method has good robustness, as it could quantitatively analyze fracture characteristics such as the width and length of cracks in samples with different rubber contents under the ultimate load.

Acknowledgment

This work was supported by the National Natural Science Foundation of China (No. U1801254/51727813/51925805) and the Project of Department of Education of Guangdong Province, China (No. 2018KZDXM060).

Data Availability

Some or all data, models, or code that support the findings of this study are available from the corresponding author upon reasonable request.

References

Akono, A.-T., Chen, J., and Kaewunruen, S. (2018). "Friction and fracture characteristics of engineered crumb-rubber concrete at microscopic lengthscale." *Construction and Building Materials*, 175, 735-745.

Barber, C. B., Dobkin, D. P., and Huhdanpaa, H. (1996). "The Quickhull algorithm for convex hulls." *ACM Trans. Math. Softw.*, 22(4), 469-483.

Boas, F., and Fleischmann, D. (2012). "CT artifacts: Causes and reduction techniques." *Imaging in Medicine*, 4.

Brahma, K. K., Sunder, R., and Dattaguru, B. (1987). "Automated estimation of fatigue crack length and closure/opening stress." *International Journal of Fatigue*, 9(1), 51-55.

Chen, Y., Zhang, Y., Yang, J., Cao, Q., Yang, G., Chen, J., Shu, H., Luo, L., Coatrieux, J. L., and Feng, Q. (2016). "Curve-Like Structure Extraction Using Minimal Path Propagation With Backtracking." *IEEE Trans Image Process*, 25(2), 988-1003.

Di, S., Jia, C., Qiao, W., Li, K., and Tong, K. (2018). "Energy Evolution Behavior and Mesodamage Mechanism of Crumb Rubber Concrete." *Advances in Materials Science and Engineering*, 2018, 1-13.

Dong, S., Han, B., Yu, X., and Ou, J. (2019). "Constitutive model and reinforcing mechanisms of uniaxial compressive property for reactive powder concrete with super-fine stainless wire." *Composites Part B: Engineering*, 166, 298-309.

Doyle, W. (1962). "Operations Useful for Similarity-Invariant Pattern Recognition." *J. ACM*, 9, 259-267.

Eldin, N. N., and Senouci, A. B. (1994). "Measurement and prediction of the strength of rubberized concrete." *Cement and Concrete Composites*, 16(4), 287-298.

Farrahi Moghaddam, R., and Cheriet, M. (2010). "A multi-scale framework for adaptive binarization of degraded document images." *Pattern Recognition*, 43(6), 2186-2198.

Fukumura, N., Li, B. C., Koyama, M., Suzuki, T., Hamada, S., Tsuzaki, K., and Noguchi, H. (2017). "Material property controlling non-propagating fatigue crack length of mechanically and physically short-crack based on Dugdale-model analysis." *Theor. Appl. Fract. Mech.*, 90, 193-202.

Germaneau, A., Doumalin, P., and Dupré, J. C. (2007). "3D Strain Field Measurement by Correlation of Volume Images Using Scattered Light: Recording of Images and Choice of Marks." *Strain*, 43(3), 207-218.

Han, Q., Yang, G., Xu, J., Fu, Z., Lacidogna, G., and Carpinteri, A. (2019). "Acoustic emission data analyses based on crumb rubber concrete beam bending tests." *Engineering Fracture Mechanics*, 210, 189-202.

Ho, A. C., Turatsinze, A., Hameed, R., and Vu, D. C. (2012). "Effects of rubber aggregates from grinded used tyres on the concrete resistance to cracking." *J. Clean Prod.*, 23(1), 209-215.

Hong, S., Kuang, C., Zhang, J., Hou, D., Zhang, J., Liu, L., and Dong, B. (2020a). "Visual analysis for microscopic cracking propagation of rubberized concrete." *Construction and Building Materials*, 265, 120599.

Hong, S., Liu, P., Zhang, J., Kuang, C., Dong, B., Luo, Q., and Liu, W. (2020b). "Interior fracture analysis of rubber-cement composites based on X-ray computed tomography and digital volume correlation." *Construction and Building Materials*, 259, 119833.

Hong, S. X., Liu, P., Zhang, J. C., Xing, F., and Dong, B. Q. (2019). "Visual & quantitative identification of cracking in mortar subjected to loads it using X-ray computed tomography method." *Cement & Concrete Composites*, 100, 15-24.

Huang, L.-K., and Wang, M.-J. J. (1995). "Image thresholding by minimizing the measures of fuzziness." *Pattern Recognition*, 28(1), 41-51.

Huang, W., Huang, X., Xing, Q., and Zhou, Z. (2020). "Strength reduction factor of crumb rubber as fine aggregate replacement in concrete." *Journal of Building Engineering*, 101346.

Jerman, T., Pernus, F., Likar, B., and Spiclin, Z. (2016). "Enhancement of Vascular Structures in 3D and 2D Angiographic Images." *IEEE Trans Med Imaging*, 35(9), 2107-2118.

Kim, M. K., Jeon, J. H., Choi, J. B., and Kim, M. K. (2020). "The effect of crack length on SIF and elastic COD for elbow with circumferential through wall crack." *Nuclear Engineering and Technology*, 52(9), 2092-2099.

Kittler, J., and Illingworth, J. (1986). "MINIMUM ERROR THRESHOLDING." *Pattern Recognition*, 19(1), 41-47.

Krajcinovic, D. (1998). "Selection of damage parameter – Art or science?" *Mechanics of Materials*, 28(1-4), 165-179.

Lam, L., Lee, S., and Suen, C. Y. (1992). "Thinning methodologies-a comprehensive survey." *IEEE Transactions on Pattern Analysis and Machine Intelligence*, 14(9), 869-885.

Li, D., Zhuge, Y., Gravina, R., and Mills, J. E. (2018). "Compressive stress strain behavior of crumb rubber concrete (CRC) and application in reinforced CRC slab." *Construction and Building Materials*, 166, 745-759.

Li, L., Ruan, S., and Zeng, L. (2014). "Mechanical properties and constitutive equations of concrete containing a low volume of tire rubber particles." *Construction and Building Materials*, 70, 291-308.

Loeffler, C. M., Qiu, Y., Martin, B., Heard, W., Williams, B., and Nie, X. (2018). "Detection and segmentation of mechanical damage in concrete with X-Ray microtomography." *Materials Characterization*, 142, 515-522.

Maki, D., Birnbaum, B. A., Chakraborty, D., Jacobs, J., Carvalho, B., and Herman, G. (1999). "Renal Cyst Pseudoenhancement: Beam-hardening Effects on CT Numbers1." *Radiology*, 213, 468-472.

Meng, Q., Zhang, M., Han, L., Pu, H., and Li, H. (2016). "Effects of size and strain rate on the mechanical behaviors of rock specimens under uniaxial compression." *Arabian Journal of Geosciences*, 9(8).

Mukherjee, S., Condron, B., and Acton, S. T. (2015). "Tubularity Flow Field—A Technique for Automatic Neuron Segmentation." *IEEE Transactions on Image Processing*, 24(1), 374-389.

Otsu, N. (1979). "A Threshold Selection Method from Gray-Level Histograms." *IEEE Transactions on Systems, Man, and Cybernetics*, 9(1), 62-66.

Ridler, T. W., and Calvard, S. (1978). "PICTURE THRESHOLDING USING AN ITERATIVE SELECTION METHOD." *Ieee Transactions on Systems Man and Cybernetics*, 8(8), 630-632.

Sfer, D., Carol, I., Gettu, R., and Etse, G. (2002). "Study of the Behavior of Concrete under Triaxial Compression." *Journal of Engineering Mechanics-asce - J ENG MECH-ASCE*, 128.

Skarżyński, Ł., and Tejchman, J. (2016). "Experimental Investigations of Fracture Process in Concrete by Means of X-ray Micro-computed Tomography." *Strain*, 52(1), 26-45.

Taha, M. M. R., El-Dieb, A. S., El-Wahab, M. A. A., and Abdel-Hameed, M. E. (2008). "Mechanical, fracture, and microstructural investigations of rubber concrete." *J. Mater. Civ. Eng.*, 20(10), 640-649.

Wang, P., Qiao, H., Zhang, Y., Li, Y., Chen, K., and Feng, Q. (2020). "Three-dimensional characteristics of steel corrosion and corrosion-induced cracks in magnesium oxychloride cement concrete monitored by X-ray computed tomography." *Construction and Building Materials*, 246, 118504.

Weng, X., Huang, Y., and Wang, W. (2019). "Segment-based pavement crack quantification." *Automation in Construction*, 105.

Xie, J. Y., Zhao, Y. T., Liu, Y. H., Su, P., Zhao, Y. F., Cheng, J., Zheng, Y. L., Liu, J., and Soc, I. C. (2019). "Topology Reconstruction of Tree-like Structure in Images via Structural Similarity Measure and Dominant Set Clustering." *2019 Ieee/Cvf Conference on Computer Vision and Pattern Recognition*, Ieee, New York, 8497-8505.

Yang, Y.-S., Wu, C.-l., Hsu, T. T. C., Yang, H.-C., Lu, H.-J., and Chang, C.-C. (2018). "Image analysis method for crack distribution and width estimation for reinforced concrete structures." *Automation in Construction*, 91, 120-132.

Yang, Z., Ren, W., Sharma, R., McDonald, S., Mostafavi, M., Vertyagina, Y., and Marrow, T. J. (2017). "In-situ X-ray computed tomography characterisation of 3D fracture evolution and image-based numerical homogenisation of concrete." *Cement and Concrete Composites*, 75, 74-83.

Yang, Z. J., Qsymah, A., Peng, Y. Z., Margetts, L., and Sharma, R. (2020). "4D characterisation of damage and fracture mechanisms of ultra high performance fibre reinforced concrete by in-situ micro X-Ray computed tomography tests." *Cement and Concrete Composites*, 106, 103473.

Zhang, J., Bekkers, E., Chen, D., Berendschot, T. T. J. M., Schouten, J., Pluim, J. P. W., Shi, Y., Dashtbozorg, B., and Romeny, B. M. t. H. (2018). "Reconnection of Interrupted Curvilinear Structures via Cortically Inspired Completion for Ophthalmologic Images." *Ieee Transactions on Biomedical Engineering*, 65(5), 1151-1165.

Zhao, Y. X., Yu, J., Hu, B. Y., and Jin, W. L. (2012). "Crack shape and rust distribution in corrosion-induced cracking concrete." *Corrosion Sci.*, 55, 385-393.

Zhou, C., Li, K., and Pang, X. (2011). "Effect of crack density and connectivity on the permeability of microcracked solids." *Mechanics of Materials*, 43(12), 969-978.

Table 1

Scanning parameters of the XCT test. (Hong et al. 2020)

Voltage (kV)	Current (μA)	Magnification (×)	Exposure time (s)	Image matrix size (voxel)	Voxel physical size (μm^3)
80	100	0.4	8	1024 × 1024 × 1000	14.2735 × 14.2735 × 14.2735

Table 2

Ultimate loads (N) of the samples with different rubber contents.

Rubber content	5%	10%	15%
Ultimate load	1850	1550	1400

Table 3

Comparison of the performances of different segmentation methods reported in the literature with that of the proposed method, regarding count, maximal width, minimal width, and the total length of detected cracks in the raw image.

Method	Count	Maximal width (μm)	Minimal width (μm)	Total length (mm)
Manually	9	98.25	43.09	67.22
Isodata (Ridler and Calvard 1978)	45	122.88	15.25	33.02
Huang et al. (Huang and Wang 1995)	34	81.47	13.51	16.33
Minimum error (Kittler and Illingworth 1986)	42	85.93	15.46	24.15
Otsu et al. (Otsu 1979)	45	122.88	15.25	32.75
Percentile (Doyle 1962)	42	85.93	15.46	24.15
Proposed method	9	94.76	37.76	66.98

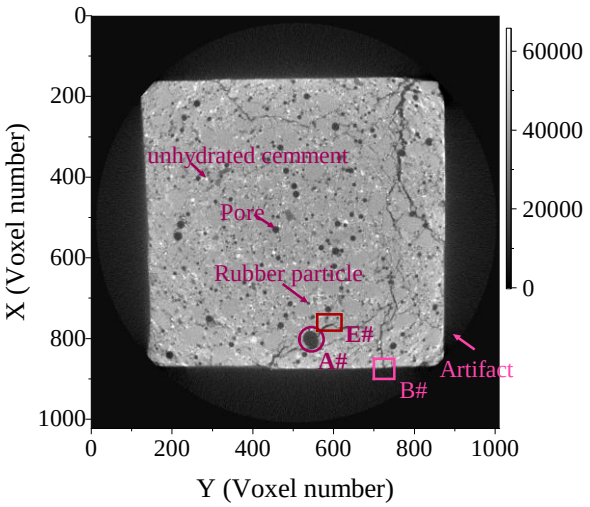

Fig. 1. Typical sectional raw XCT (X-ray computed tomography) image of rubber concrete

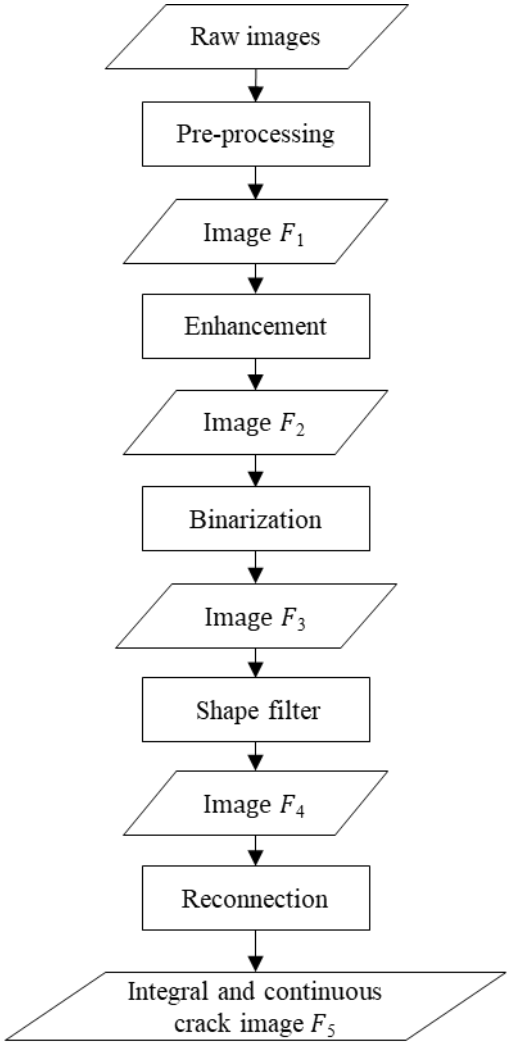

Fig. 2. Schematic diagram of the proposed method

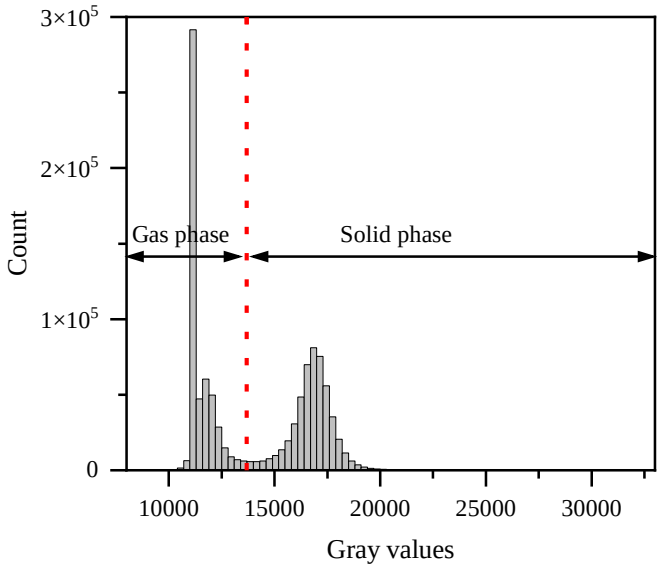

Fig. 3. Histogram of the gray values of the XCT image in Fig. 1

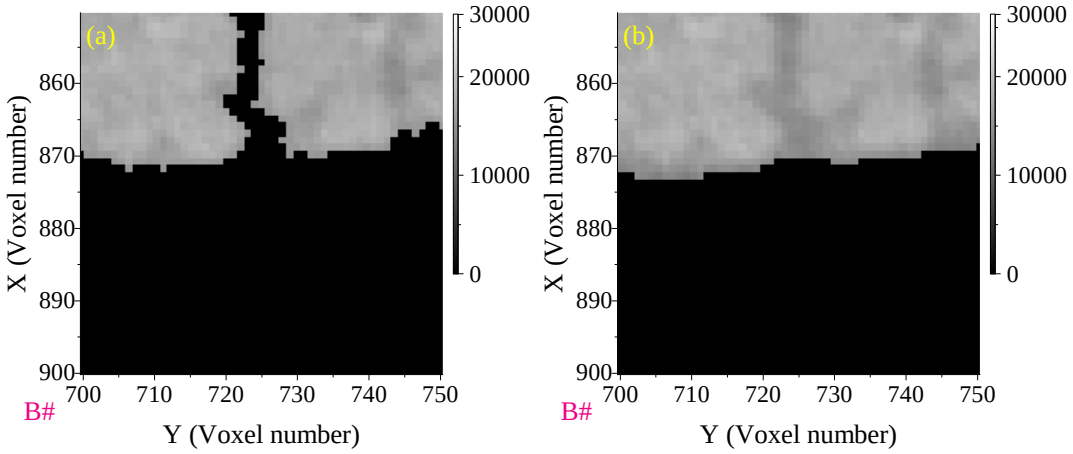

Fig. 4. Boundary detecting result: (a) detecting result on region B# in Otsu's method (Otsu 1979); (b) boundary detecting result on region B# in the preprocessing method.

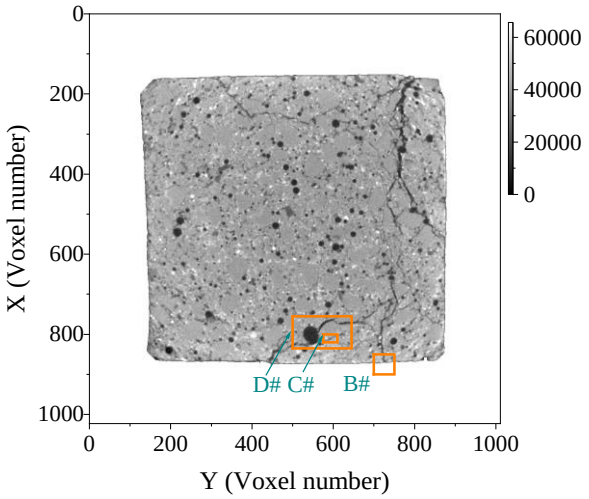

Fig. 5. Preprocessing result of the raw XCT image in Fig. 1

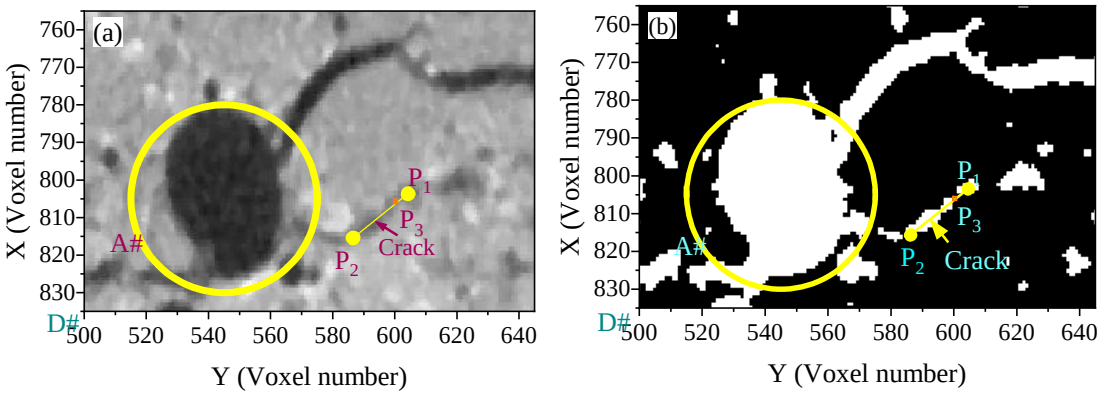

Fig. 6. Effect of the unevenness of crack gray values: (a) area D# in Fig. 5; (b) binary result of (a) obtained using the adaptive Otsu's method (Farrahi Moghaddam and Cheriet 2010).

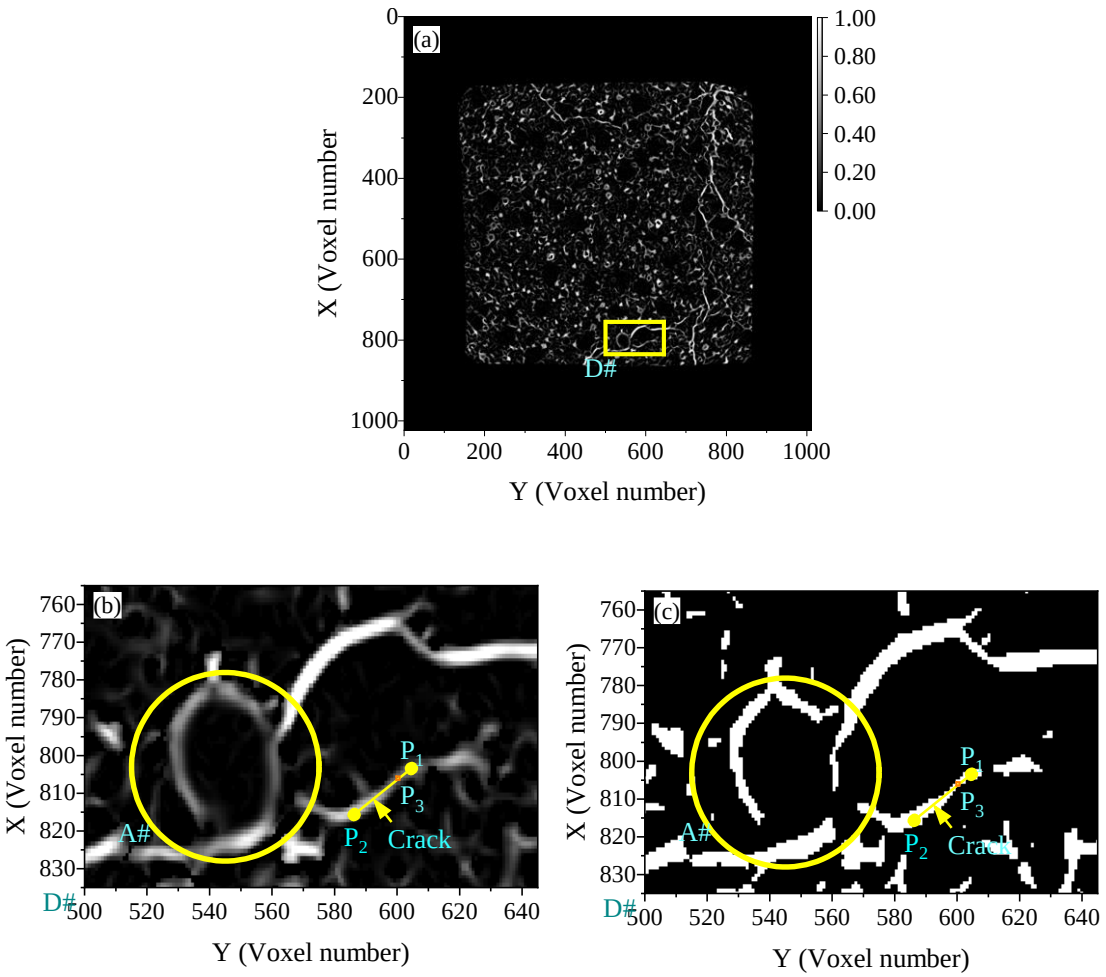

Fig. 7. Enhanced results: (a) the result of the enhancement on the image in Fig. 5; (b) area D# in (a); (c) binary result of (b) obtained using the adaptive Otsu's method (Farrahi Moghaddam and Cheriet 2010).

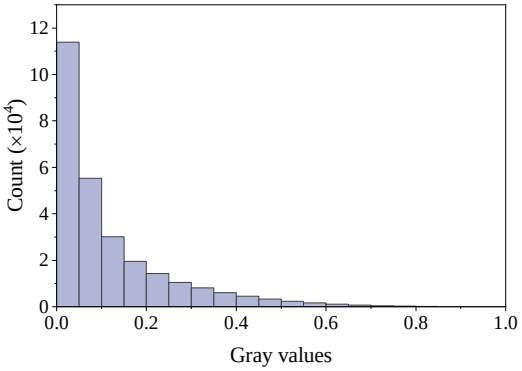

Fig. 8. Histogram of the gray values in the enhanced image in Fig. 7(a)

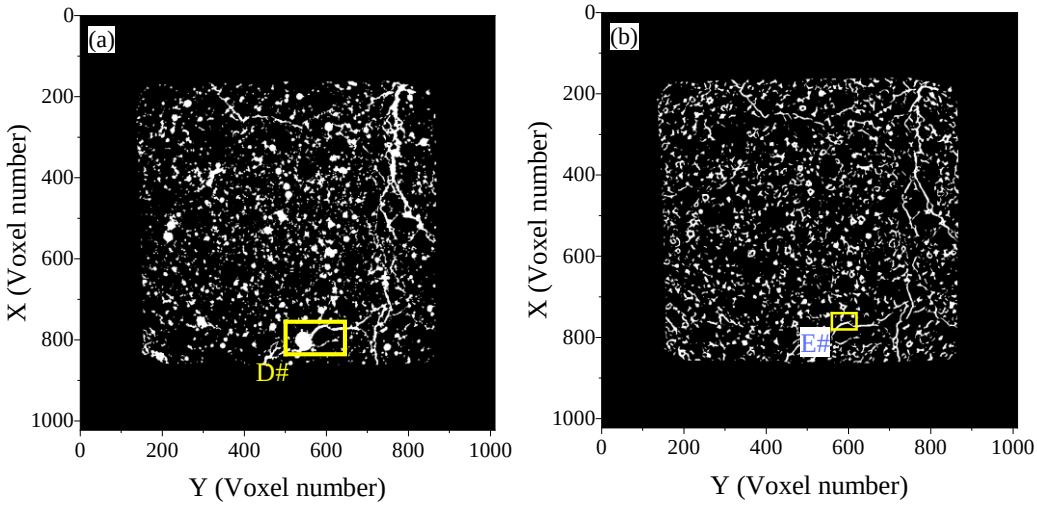

Fig. 9. Binary results: (a) image obtained by applying Otsu's method to Fig. 1; (b) image obtained by applying adaptive Otsu's method (Farrahi Moghaddam and Cheriet 2010) with a window size of 15 pixels to Fig. 7(a).

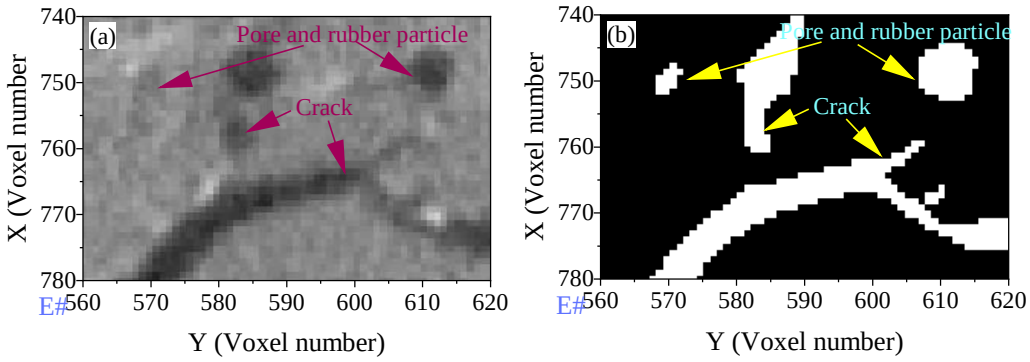

Fig. 10. Local binary results in area E#: (a) raw area E# of Fig. 1; (b) area E# in Fig. 9(a).

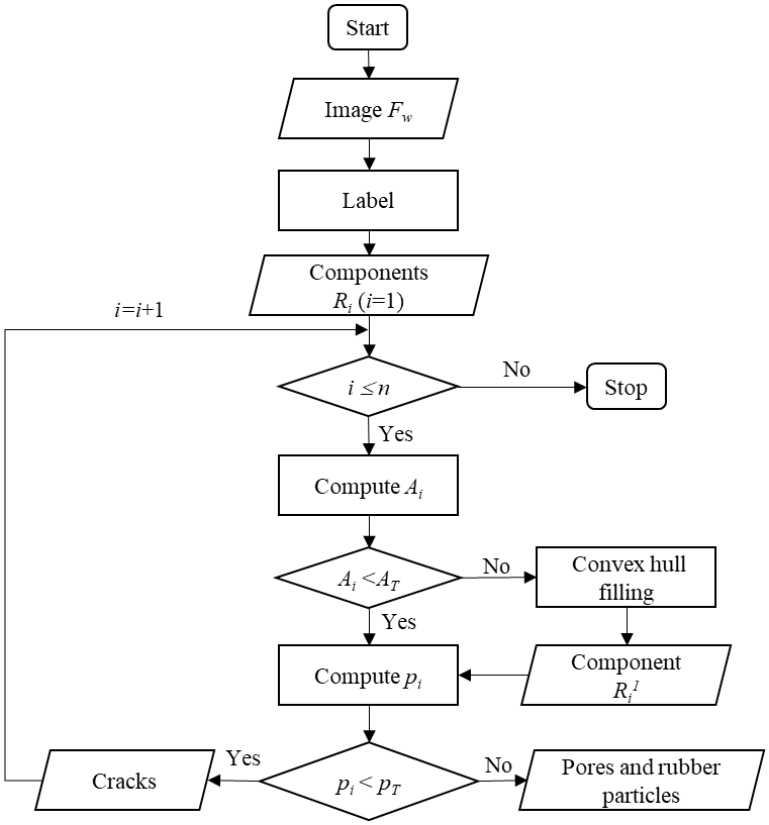

Fig. 11. Procedure of the shape filter

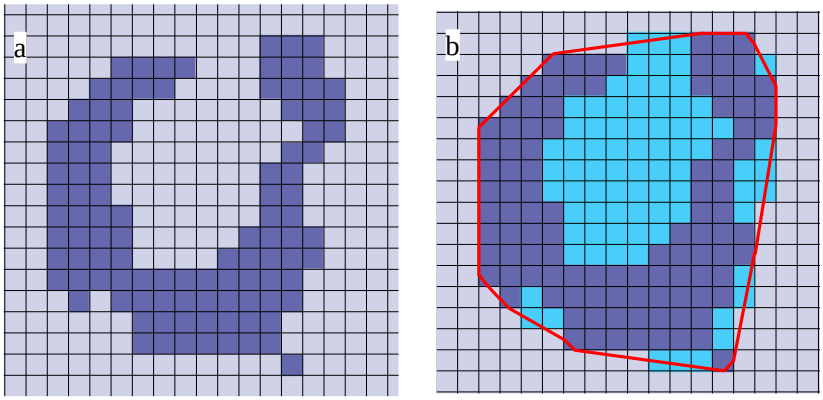

Fig. 12 Schematic diagram of the minimum external convex polygon filling of a hollow component: (a) a hollow rounded component with a notch; (b) the filling result.

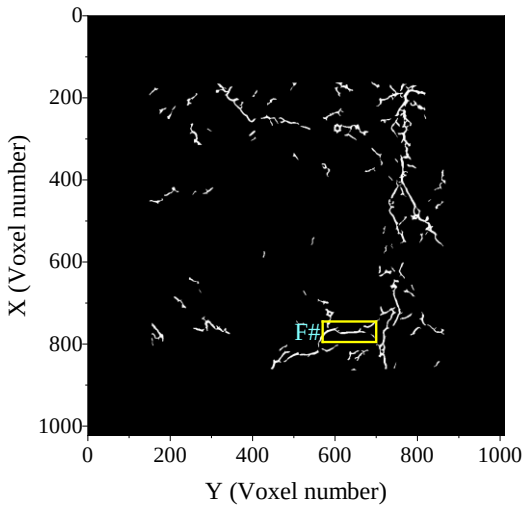

Fig. 13. Cracks obtained by the shape filter

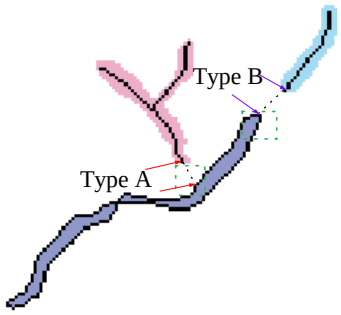

Fig. 14. Two types of discontinuities between the disjoint components. Type A and type B can be resolved by connecting the endpoint of the center lines of one component to the boundary line of another component.

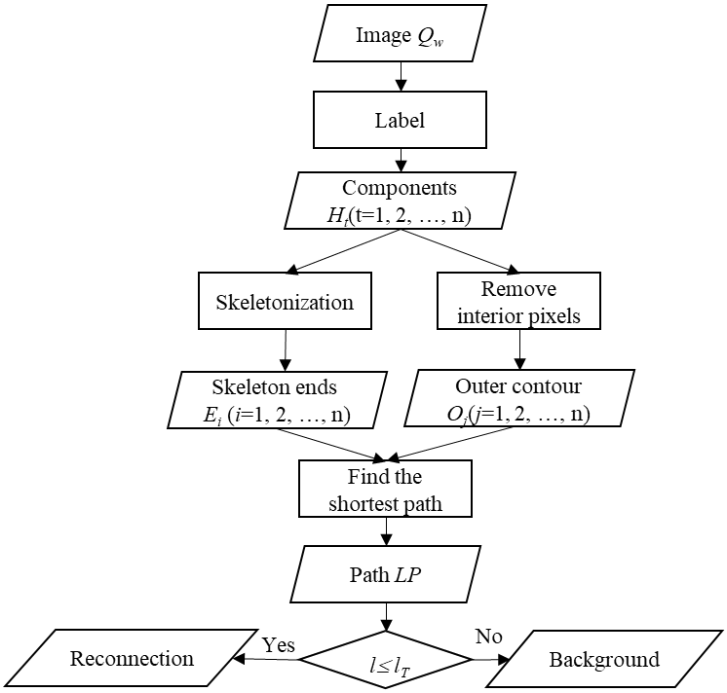

Fig. 15. Procedure of the reconnecting algorithm

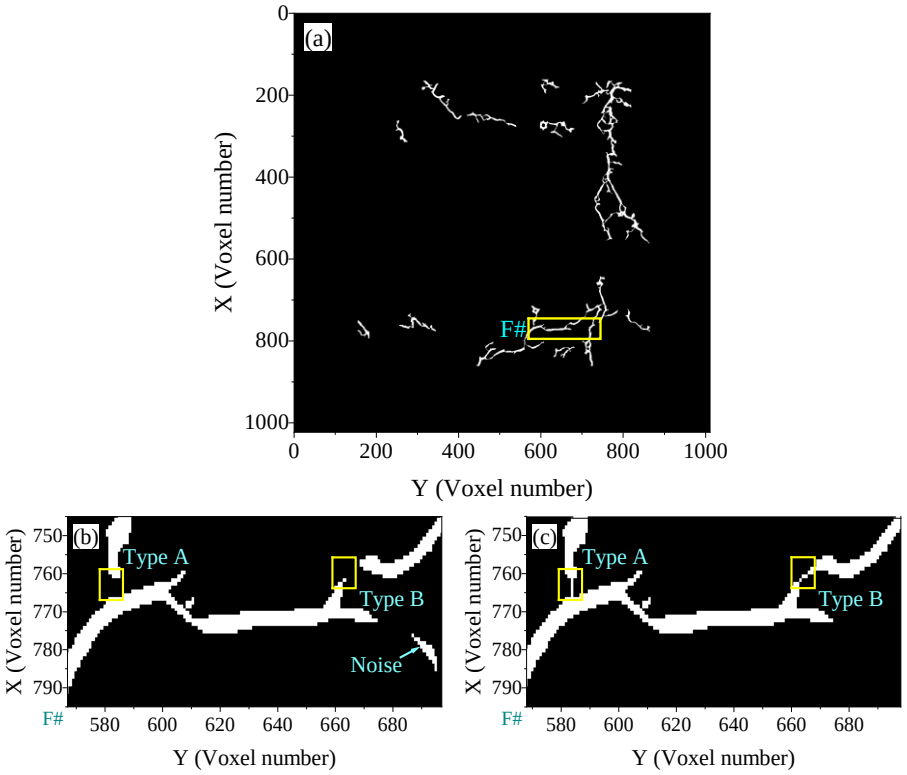

Fig. 16. Cracks after reconnecting and denoising: (a) final cracks image; (b) area F# in (a); (c) reconnected cracks in area F#.

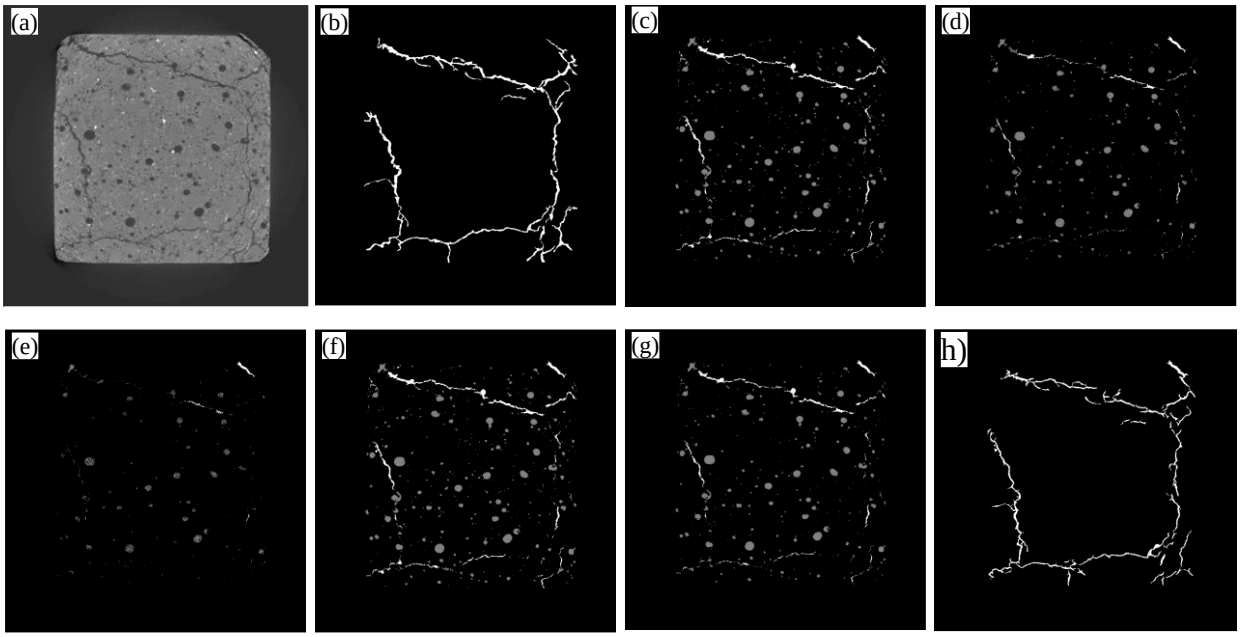

Fig. 17. Image segmentation results obtained with different methods: (a) raw image; (b) manually marked cracks; (c) ISODATA algorithm (Ridler and Calvard 1978); (d) Huang et al.'s method(Huang and Wang 1995); (e) minimum error thresholding algorithm (Kittler and Illingworth 1986); (f) Otsu et al.'s method(Otsu 1979); (g) percentile (Doyle 1962); (h) the propose method. (Gray parts in (c)–(e) indicate pores with a roundness index higher than 0.7. The images (a) have a size of 1024×1024×1 voxels.)

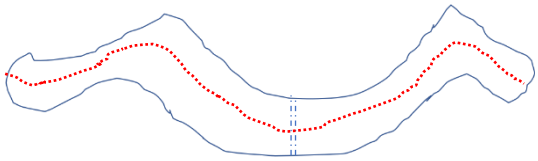

Fig. 18. Schematic diagram for crack width calculation

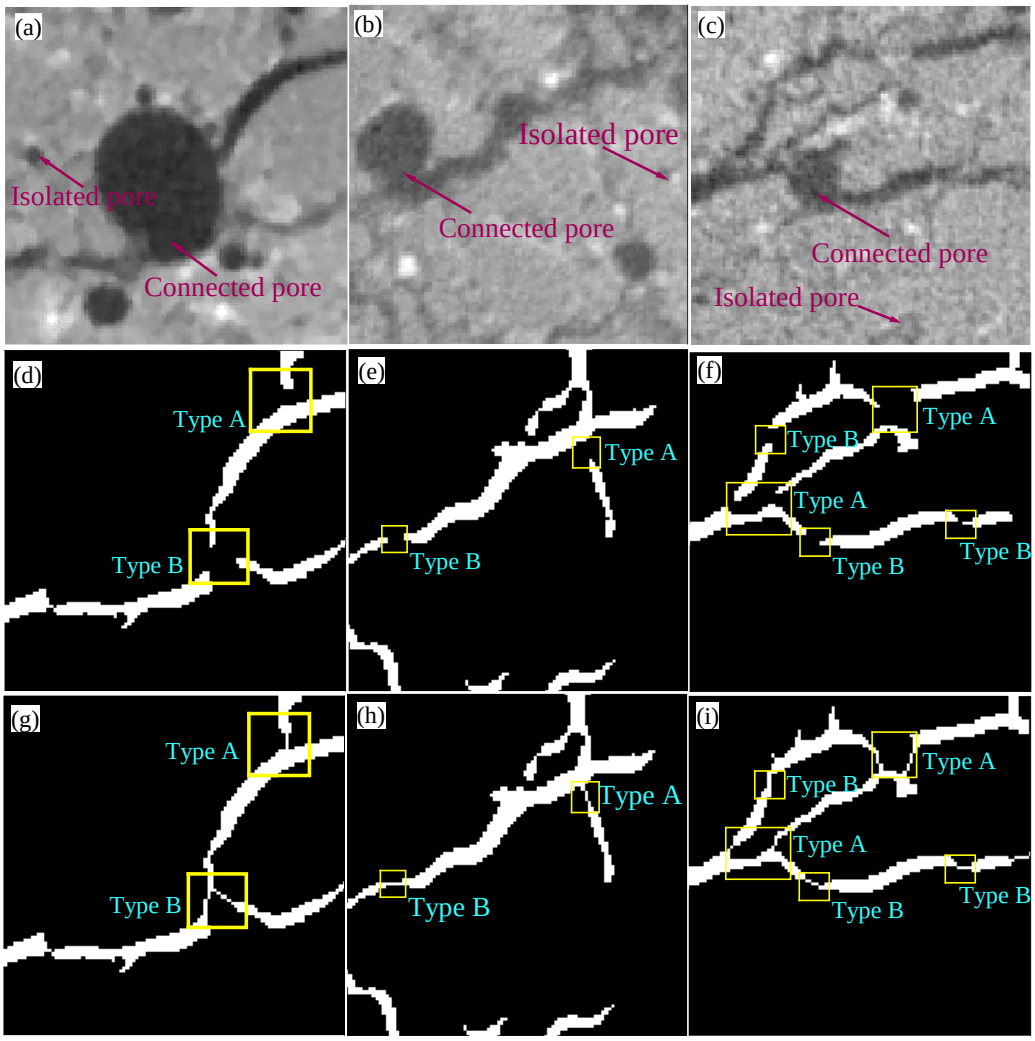

Fig. 19. Performance on different uneven images: (a)–c) selected three typical uneven raw image fragments; (d)–(f) interrupted cracks detected without reconnection; (g)–(i) detected cracks after reconnection. (The images in (a)-(i) have a size of 80×80×1 voxels.)

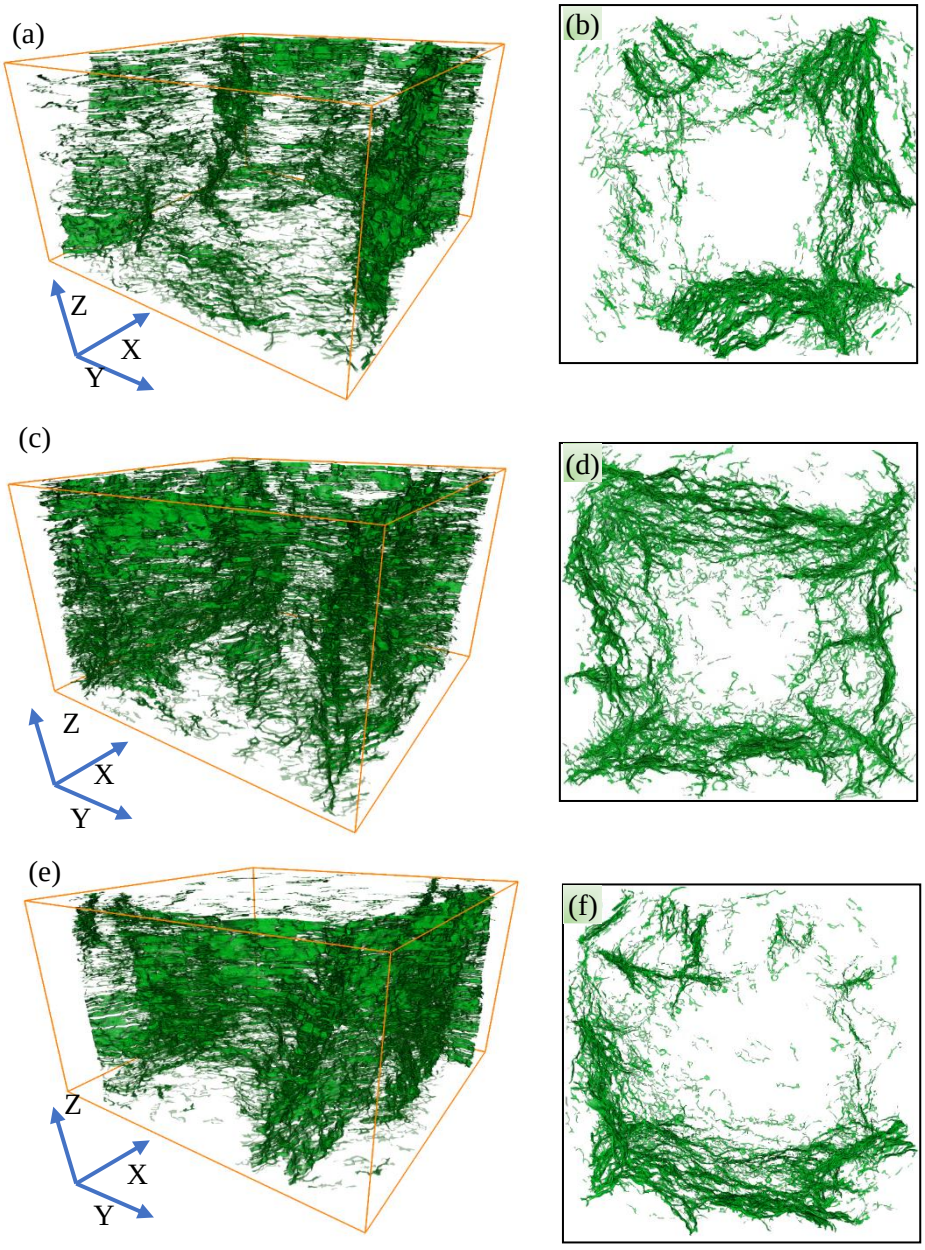

Fig. 20. Three-dimensional diagram and XY sectional projection of cracks in rubber concrete samples with different contents after ultimate loading: (a) three-dimensional diagram of cracks in the sample with 5% rubber content; (b) XY sectional projection of cracks in the three-dimensional diagram in (a); (c) three-dimensional diagram of cracks in the sample with 10% rubber content; (d) XY sectional projection of cracks in the three-dimensional diagram in (c); (e) three-dimensional diagram of cracks in the sample with 15% rubber content; (f) XY sectional projection of cracks in the three-dimensional diagram in (e). (The 3D images in (a), (c), and (e) have a size of 801×813×468 voxels. The 2D images in (b), (d), and (f) have a size of 801×813 pixels.)

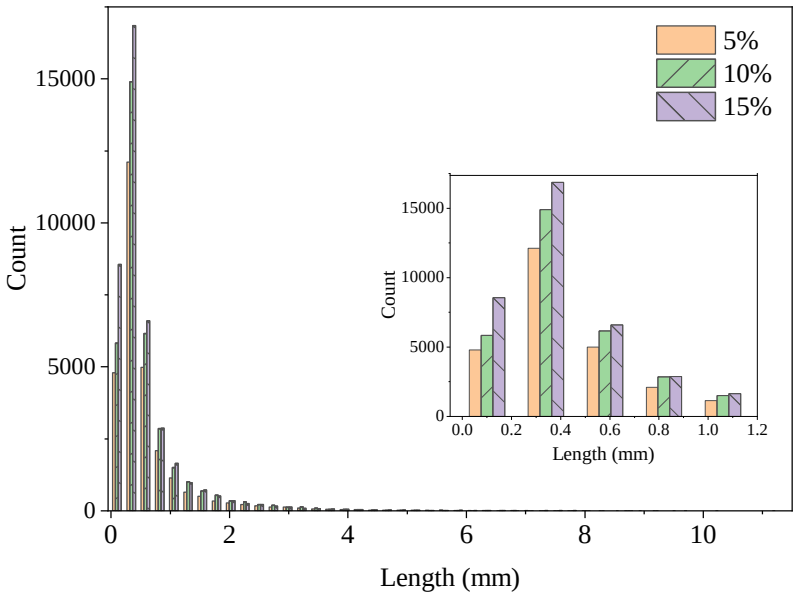

Fig. 21. Distribution of cracks with different lengths in samples with different rubber contents.

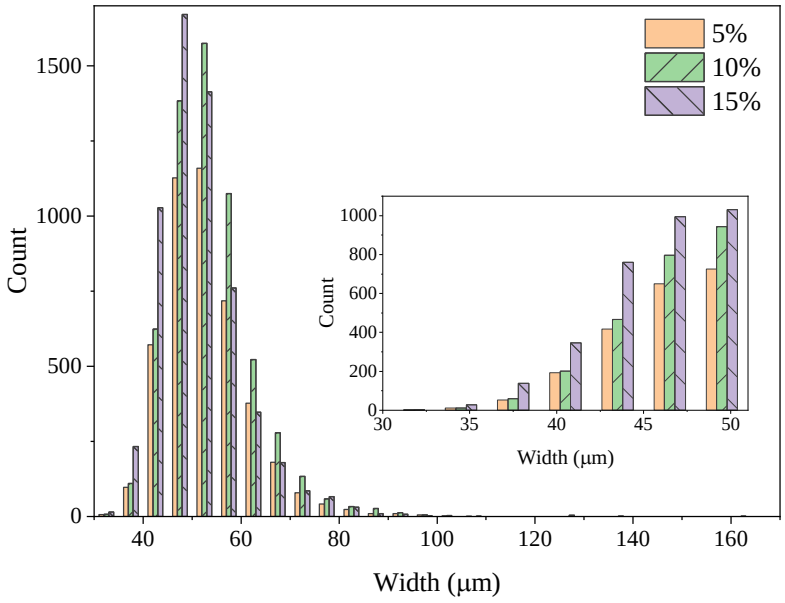

Fig. 22. Distribution of cracks with different widths in samples with different rubber contents.